

2009 Special Issue

Dopamine-modulated dynamic cell assemblies generated by the GABAergic striatal microcircuit

Mark D. Humphries*, Ric Wood, Kevin Gurney

Adaptive Behaviour Research Group, Department of Psychology, University of Sheffield, S10 2TN, UK

ARTICLE INFO

Article history:

Received 12 February 2009
Received in revised form 19 June 2009
Accepted 14 July 2009

Keywords:

Striatum
Parkinson's disease
Action selection
Large-scale models
Izhikevich neuron model

ABSTRACT

The striatum, the principal input structure of the basal ganglia, is crucial to both motor control and learning. It receives convergent input from all over the neocortex, hippocampal formation, amygdala and thalamus, and is the primary recipient of dopamine in the brain. Within the striatum is a GABAergic microcircuit that acts upon these inputs, formed by the dominant medium-spiny projection neurons (MSNs) and fast-spiking interneurons (FSIs). There has been little progress in understanding the computations it performs, hampered by the non-laminar structure that prevents identification of a repeating canonical microcircuit. We here begin the identification of potential dynamically-defined computational elements within the striatum. We construct a new three-dimensional model of the striatal microcircuit's connectivity, and instantiate this with our dopamine-modulated neuron models of the MSNs and FSIs. A new model of gap junctions between the FSIs is introduced and tuned to experimental data. We introduce a novel multiple spike-train analysis method, and apply this to the outputs of the model to find groups of synchronised neurons at multiple time-scales. We find that, with realistic *in vivo* background input, small assemblies of synchronised MSNs spontaneously appear, consistent with experimental observations, and that the number of assemblies and the time-scale of synchronisation is strongly dependent on the simulated concentration of dopamine. We also show that feed-forward inhibition from the FSIs counter-intuitively increases the firing rate of the MSNs. Such small cell assemblies forming spontaneously only in the absence of dopamine may contribute to motor control problems seen in humans and animals following a loss of dopamine cells.

© 2009 Elsevier Ltd. All rights reserved.

1. Introduction

The striatum is a large subcortical nucleus that forms the principal input structure of the basal ganglia. Diseases that directly affect the striatum or its primary afferents – such as Huntington's or Parkinson's disease – lead to profound deficits in motor control. In particular, loss of dopamine cells in Parkinson's disease and its animal models leads to motor symptoms of rigidity, akinesia, and tremor (Ferro et al., 2005; Kirik, Rosenblad, & Bjorklund, 1998; Schwarting & Huston, 1996), and the striatum is the main locus of dopamine's action, containing the highest density of dopamine receptors in the vertebrate brain (Dawson, Gehlert, McCabe, Barnett, & Wamsley, 1986; Hurd, Suzuki, & Sedvall, 2001; Richtand, Kelsoe, Segal, & Kuczenski, 1995). Moreover, an intact dopamine system also seems to be critical for many forms of learning (Ferro et al., 2005; Whishaw & Dunnett, 1985), consistent with reported correlations between dopamine cell firing and the prediction error required by reinforcement learning theories (Redgrave

& Gurney, 2006; Schultz, 2007). An intact striatum is similarly required for successful acquisition of many instrumental conditioning tasks (Yin & Knowlton, 2006). An understanding of the striatum's computational operation would thus shed light on a fundamental contributor to both motor control and learning.

Within the striatum lies a complex, predominantly GABAergic, microcircuit (Bolam et al., 2006). Medium spiny projection neurons (MSNs) are the only output neurons and comprise up to 95% of the cell population in rats, with GABAergic and cholinergic interneurons forming most of the remaining cell population. Despite their comparatively small number, the GABAergic fast-spiking interneurons (FSIs), in particular, exert a very strong influence on the MSNs (Koos & Tepper, 1999), receive input from similar sources, and are interconnected by both chemical synapses and gap junctions. Dopamine has multiple effects on these neuron types, via multiple receptor types: indeed, the exact effects of dopamine receptor activation on the MSN have been much debated (Surmeier, Ding, Day, Wang, & Shen, 2007). Seemingly ideal for underpinning its multiple functional roles, the striatum receives massive convergent input from the neocortex, thalamus, hippocampal formation, and amygdala (Glynn & Ahmad, 2002; Groenewegen, Wright, Beijer, & Voorn, 1999; McGeorge & Faull, 1989; Smith, Raju, Pare, &

* Corresponding author. Tel.: +44 7932 780 235.

E-mail address: m.d.humphries@sheffield.ac.uk (M.D. Humphries).

Sidibe, 2004), and dopamine modulates the striatal neurons' responses to them.

Despite, or perhaps due to, this complexity of structure and input, there are few well-quantified theories of the striatum's computational role. Many theories of striatal-specific or global basal ganglia function draw explicit attention to the role of the inhibitory local MSN collaterals as a substrate for competitive dynamics (e.g. Beiser & Houk, 1998; Frank, 2005; Pennartz, Groenewegen, & da Silva, 1994; Wickens, Alexander, & Miller, 1991), whether that competition be labelled 'decision making', 'motor program selection' or 'pattern classification'. Wickens and colleagues' domain hypothesis is the most developed, and proposes that the basic computational element of the striatum is the set – or "domain" – of all MSNs that are mutual inhibitory (see e.g. Alexander & Wickens, 1993; Wickens et al., 1991; Wickens, Kotter, & Alexander, 1995). In simulation, they have shown that winner-takes-all like competition occurs within a single domain, while winners-share-all dynamics (multiple active neurons) occur in networks composed of multiple overlapping domains (Alexander & Wickens, 1993; Wickens et al., 1991). Similar results have been obtained in analytical studies of general mutually inhibitory neural networks (Fukai & Tanaka, 1997).

All such theories of competitive dynamics are faced by the problems that the inhibition provided by the local MSN collaterals is weak (Czubayko & Plenz, 2002; Jaeger, Hitoshi, & Wilson, 1994; Koos, Tepper, & Wilson, 2004; Taverna, van Dongen, Groenewegen, & Pennartz, 2004; Tunstall, Oorschot, Kean, & Wickens, 2002), so that a single MSN is only contacted by between 12%–18% of MSNs in its dendritic field (Tepper, Koos, & Wilson, 2004), and that *mutual inhibition* is the exception rather than rule (Tepper et al., 2004; Tunstall et al., 2002).

Some theories do predict such weak connections. Bar-Gad, Morris, and Bergman (2003) have proposed that the striatum compresses information relayed to it from the cortex, transmitting back the compressed version via the basal ganglia output nuclei. They noted that the two layer network formed by the striatum and the output nuclei can be mapped to standard neural network implementations of principal components analysis, and that these require weak correlation in a layer corresponding to the striatum. While an interesting hypothesis, this mapping does not account for the microcircuit of the striatum, or the effects of the numerous neuromodulators within it. Other models of the whole basal ganglia circuit do not rely on the local collaterals within the striatum for their computations, rather proposing that the striatum is both an integrator of diverse cortical information and a filter on weak cortical inputs, as the first stage of an input selection mechanism implemented by the whole basal ganglia (as opposed to just the striatum), (Gurney, Prescott, & Redgrave, 2001; Humphries, Stewart, & Gurney, 2006) – but these models also do not account for the striatal microcircuit.

Our aim is to find out what computations can be supported by the intrinsic circuitry of the striatum, what – if any – "basic computational elements" exist, and develop computational theories of function on this basis. In particular, we wish to understand the role of the dominant GABAergic circuits of the striatum: the rare, but powerful, FSIs, and the weak, asymmetrical, but comparatively plentiful MSN local collaterals. Understanding the contribution of all the striatum's elements ideally requires large-scale models (Djurfeldt, Ekeberg, & Lansner, 2008) that replicate the neuron types, numbers, and connectivity at a one-to-one scale. Such models can give deep insight into the role of each neuron class in local circuit dynamics.

The purpose of this paper is twofold. First, we draw together, for the first time, a series of techniques we have developed for leveraging anatomical and physiological constraint data, some of which promise general applicability (beyond the striatum) in microcircuit

construction: (1) a powerful computational neuroanatomy method for extracting the best connectivity statistics from impoverished data; (2) the development of reduced models for dopamine modulation of striatal neurons, which replicate the output of detailed compartmental models; and (3) a rigorous method for spike generation which allows good approximation to cortical input. We add to these here by introducing: (1) a gap junction model tunable to known membrane properties; (2) a principled method for parameterising the spike generation tool based on anatomical and physiological data; and (3) a novel method for detecting patterns in multi-unit activity at multiple time-scales, with general applicability to simulation or experimental data.

Second, we begin the identification of computational elements within the striatum, and examine how these might support hypotheses for competitive dynamics underpinned by the GABAergic neurons of the striatum. Specifically, we construct a three-dimensional model of the striatal microcircuit's connectivity, and instantiate this with our dopamine-modulated neuron models of the MSNs and FSIs. We apply our multiple spike-train analysis to the outputs of this model to find groups of synchronised neurons at multiple time-scales. We then show that, with realistic *in vivo* background input, small assemblies of synchronised MSNs spontaneously appear, consistent with experimental observations (Carrillo-Reid et al., 2008), and that the number of assemblies and the time-scale of synchronisation is strongly dependent on the simulated concentration of dopamine.

2. Creating the striatal microcircuit

Building large-scale models at up to 1:1 scale, neuron for neuron, is an ambitious aim. In particular, as recognised by the Blue Brain Project (Markram, 2006), these models are severely limited by the need for accurate connectivity. There is a wealth of studies showing how the structure of a network is a strong determinant of its dynamics (see e.g. Galan, 2008; Kwok, Jurica, Raffone, & van Leeuwen, 2007; Nishikawa, Motter, Lai, & Hoppensteadt, 2003), and that the typical fall-back of completely regular or random networks give false impressions about both synchronisation and stability (see especially Lago-Fernandez, Huerta, Corbacho, & Siguenza, 2000; Watts & Strogatz, 1998). It is thus imperative that we begin from as accurate a network structure as possible.

2.1. The striatal microcircuit

First, we specify the GABAergic microcircuit of the striatum (Tepper et al., 2004). Fig. 1 shows its complete set of connections and neuron types; these are intermingled throughout the non-laminar structure of the striatum. The MSNs number around 2,790,000 in the rat, with a (shrinkage-corrected) density of 85,000 per mm³ (Oorschot, 1996). Various estimates have placed this total as anything up to 95% of all neurons in the striatum (Gefen & Wilson, 1996), though a figure of 90% is more commonly quoted (Kawaguchi, Wilson, Augood, & Emson, 1995). The MSNs can be split into two populations on the basis of their dominant expression of either the D1 or D2 dopamine receptor, and these populations are of roughly equal size. In addition to their long axonal projections to targets in the pallidum (D2 MSNs) and substantia nigra pars reticulata (D1 MSNs), both types have extensive local axon collaterals, which ramify in approximately the same volume as the parent neurons' dendrites.

The physiological class of FSIs seem to correspond to the class of parvalbumin-immunoreactive interneurons (Kawaguchi, 1993), and these comprise around 3%–5% of the striatal cell population in the rat (Kawaguchi et al., 1995). Their axons remain wholly in the striatum, and target both MSNs (Koos & Tepper, 1999) and other FSIs (Kita, Kosaka, & Heizmann, 1990). In addition,

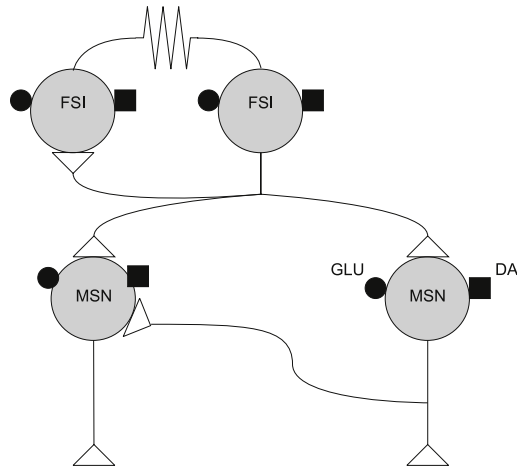


Fig. 1. The striatal GABAergic microcircuit studied in this paper. Primary input to the striatum comes from glutamatergic (GLU: ●) fibres originating in the neocortex, thalamus, hippocampal formation and amygdala, and dopaminergic (DA: ■) fibres originating in the hindbrain dopamine cell bands. All striatal axo-dendritic connections (Δ) are GABAergic and hence inhibitory. The fast-spiking interneurons (FSIs) can form dendro-dendritic gap junctions between them. The medium spiny neuron (MSN) population can be divided in two on the basis of the dominant dopamine receptor (D1 or D2) they express.

there are dendro-dendritic gap junctions between FSIs (Koos & Tepper, 1999). Both MSNs and FSIs receive glutamatergic input from cortical and thalamic sources, and dopaminergic input from the hindbrain dopamine cell bands.

We focus on this microcircuit as the neuron types are the best characterised (Tepper et al., 2004), but hence omit at least two other physiological classes of interneuron found in the striatum. The long-lasting hyperpolarisation class corresponds to the large aspiny cholinergic interneurons (Kawaguchi, 1993). We are focusing here on the short time-scale dynamics in the striatum, which are thought to be dominated by the GABAergic elements (Mallet, Le Moine, Charpier, & Gonon, 2005; Tepper et al., 2004). Future work on this circuit will incorporate the cholinergic interneurons, as they may play a role in setting the dynamic state of the striatal network (Wickens et al., 1991) and their regulation of dopamine release affects plasticity at cortico-striatal synapses (Wang et al., 2006; Zhou, Wilson, & Dani, 2002). The low-threshold spiking class corresponds to the interneurons that co-express nitric oxide, somatostatin, and neuropeptide Y (Kawaguchi, 1993; Kawaguchi et al., 1995); this class may also express GABA (Kubota & Kawaguchi, 2000). The FSIs probably dominate MSN behaviour, as they form far more synapses on somas (Kubota & Kawaguchi, 2000), whereas the low-threshold spiking neurons may form an inhibitory network between the cholinergic interneurons (Sullivan, Chen, & Morikawa, 2008).

2.2. The neuroanatomical model

We developed a novel computational neuroanatomy method to build a three-dimensional model of the striatum that is as accurate as possible given current neuroanatomical data (Wood, Humphries, & Gurney, 2007). The strength of this method is that it can be updated and re-run each time new relevant data becomes available. We review the outline of the method and the results essential for reconstructing the network used here.

Our approach builds on the underlying assumption that the probability of connection between a given pair of neurons is proportional to the distance between the cell bodies, and the overlap of their neurites at that distance. For a standard axo-dendritic synapse, the probability of connection is thus proportional to the joint volume occupied by both the axonal field

Table 1
Parameters for the expected number of contacts between neuron pairs.

Connection	α	β	γ
MSN-MSN	0.5567	0.1212	0.008
FSI-MSN	0.5528	0.1184	0.0082
FSI-FSI	0.2216	0.083	0.008
FSI gap	0.2892	0.0099	0.0132

of the source neuron and the dendritic field of the target neuron. However, like much neural tissue, detailed data on the dendrites, axons, and their three-dimensional structure were not available for the MSNs and FSIs.

We thus developed the method outlined in Fig. 2. This method relies on developing stochastic growth models for the dendrites and axons of both MSNs and FSIs. For the dendritic trees, we used an existing growth algorithm (Burke, Marks, & Ulfhake, 1992) and found its parameters using a genetic algorithm search of a fitness space defined by known parameters (e.g. number of branch points) of the neuron type's dendritic tree. For the axon, which has a simpler structure, we created our own growth algorithm based on known properties of MSN and FSI axons. By creating models for the dendrite and axon structure, we had a full set of data on the dendritic branches and axons at each distance from the soma, including their approximate volume. Using the growth algorithms, we produced a large number of dendritic trees and axons to estimate the expected neurite volume.

Based on this, we could then compute the expected volume of a sphere that was occupied by dendrite (or axon) at a given distance from the cell body. Both MSNs (Wilson & Groves, 1980; Zheng & Wilson, 2002) and FSIs (Kawaguchi, 1993; Koos & Tepper, 1999) have approximately spherical dendritic and axonal fields, and so we could compute the expected amount of neurite in all directions – effectively modelling a mean-field dendrite or axon. Then, in turn, we could compute the expected volume of overlap between the spherical fields given the distance between cell bodies for each connection type. For every $1 \mu\text{m}^3$ voxel in this overlapping volume, we computed the probability of its occupancy by both neurites (axon and dendrite or dendrite and dendrite, depending on the connection type) and thus the probability of a potential contact. Summing over all voxels in the overlapping volume thus gave us the expected number of contacts for each distance between cell bodies.

2.3. Construction of the network

We found that the expected number of contacts between two neurons, as a function of the distance d_s between the two somas, was well fitted by the truncated power law

$$E_c(d_s) = \alpha d_s^{-\beta} e^{-d_s \gamma}, \quad (1)$$

for every connection type. Table 1 gives the specific parameter values for each of the four connection types in the striatal GABAergic microcircuit: between MSNs formed by the local axon collaterals synapsing on MSN dendritic trees; FSI axonal connections on MSN dendritic trees; FSI axonal connections on FSI dendritic trees; and gap junctions between FSI dendritic trees. Fig. 2f shows the four resulting functions.

We use these functions to construct our striatal network. First, we specify the three dimensions of our simulated region of the striatum. The resulting volume $V \text{ mm}^3$ defines the number of neurons (see Section 2.1): given the 85,000 MSNs per mm^3 (Oorschot, 1996) we get $V \times 85,000$ MSNs, and 3% of this is added as FSIs (Kawaguchi et al., 1995). All neurons are then randomly assigned a three-dimensional position within the defined volume, with a minimum distance of $10 \mu\text{m}$ enforced.

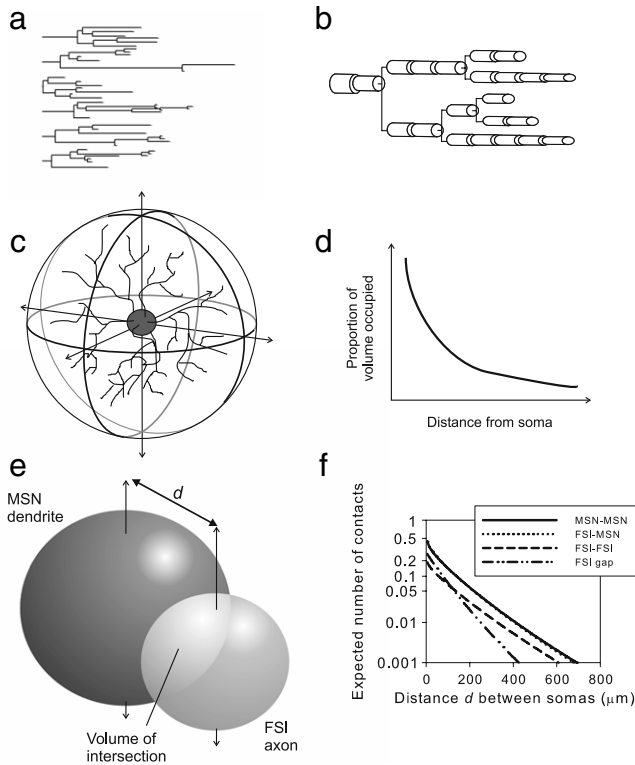


Fig. 2. Anatomy model construction. (a) We create complete dendrograms using stochastic algorithms, bounded by known properties of the dendrites and axons. This example shows all six dendrites of the complete dendrogram for one MSN. (b) Each segment of each branch is modelled as a cylinder, whose diameter tapers with distance from the soma – summing over all branches gives the total volume of dendrite (or axon) at each distance from the soma. (c) We then compute the proportion of spherical volume occupied by dendrite (or axon) at each distance from the soma. (d) Expected values for occupied volume are computed over many repetitions of the growth algorithm. The result is a continuous function of volume occupancy for each dendrite and axon type. (e) Volume of intersection of all dendrite and axon fields found for each distance between somas; volume discretised into $1 \mu\text{m}^3$ voxels. (f) For each voxel, given its distance from the respective somas, we compute the probability of intersection between fields (dendrite-axon or dendrite-dendrite) from volume occupancy functions (in panel d). We then sum over all probabilities to get the expected number of contacts between neuron pairs as a function of distance between their somas. These are all functions of the form (1), with parameters given in Table 1; we use these functions to construct our network.

For all pairs of neurons with potential connections we then apply (1) with the appropriate parameters from Table 1 for the connection type (MSN-MSN local collaterals, FSI-MSN axo-dendritic, FSI-FSI axo-dendritic, FSI-FSI dendro-dendritic gap junctions). As shown in Fig. 2f, the expected number of connections was always much less than one, and so we used these functions as giving the *probability* of connection given the distance between somas – then the total number of such connections in a sufficiently large network would yield the same expected connection function. We have successfully used this to build and run models up to 1mm^3 , though the models we use here are kept small so that a thorough analysis of the outputs remains tractable.

3. Model neurons

The model striatal network forms the basis for our study of its dynamics. If we are to build at such scales, we require individual neuron models that are simple enough to be computationally tractable, but sufficiently complex to capture key membrane properties that contribute to the characteristic behaviour of a neuron species. Our neuron model of choice is the recent canonical spiking model of Izhikevich (2007), which has been employed in

some notably large-scale models (Izhikevich, Gally, & Edelman, 2004).

We previously extended these model neurons by incorporating dopaminergic modulation of intrinsic and synaptic ion-channels, which we review below. In this paper we extend the model further by introducing a model of gap junctions between FSIs and tune parameter values to data from gap-junction coupled cortical FSIs.

3.1. Reduced models of striatal neurons

In his recent book, Izhikevich (2007) gives a biophysical form of his canonical model for spike generation. Given that v is the membrane potential, and u is the contribution of the neuron class's dominant slow current, we have

$$C\dot{v} = k(v - v_r)(v - v_t) - u + I \quad (2)$$

$$\dot{u} = a[b(v - v_r) - u], \quad (3)$$

with reset condition

$$\text{if } v \geq v_{\text{peak}} \text{ then } v \leftarrow c, u \leftarrow u + d,$$

where C is capacitance, v_r and v_t are the resting and threshold potentials, I is a current source, a is a time constant, and c is the reset potential (i.e. the value of the membrane potential immediately after an action potential is fired). Parameters k and b are derived from the I - V curve of the neuron and d is tuned to achieve the desired spiking behaviour. We solve all neuron models using the forward Euler method with a time-step of 0.01ms – this small time-step is necessary because of the fast dynamics of the FSI (Humphries & Gurney, 2007).

3.1.1. Dopamine-modulated MSNs

Izhikevich (2007) provided parameter values that modelled a MSN response to current injection. We introduced a framework for reformulating and extending this model to replicate the output of a detailed dopamine-modulated multi-compartment model (Moyer, Wolf, & Finkel, 2007) – see (Humphries et al., submitted for publication) for details. The MSN population is split in two by the expression of the dominant dopamine receptor type (D1 or D2). These receptors have different effects on both intrinsic and synaptic ion channels (see Surmeier et al., 2007, for review). We express the relative level of dopamine receptor occupancy by the parameters ϕ_1 (for D1) and ϕ_2 (for D2), normalised to the interval $[0,1]$. We add dopaminergic modulation of intrinsic ion channels in D1 MSNs by extending (2) to

$$C\dot{v}_{D1} = k(v_{D1} - v_r)(v_{D1} - v_t) - u + I + \phi_1 g_{DA}(v_{D1} - E_{DA}), \quad (4)$$

where the term $\phi_1 g_{DA}(v_{D1} - E_{DA})$ is sufficient to simulate the hyperpolarising effect of D1 activation when at an already hyperpolarised membrane potential, and the depolarising effect of D1 activation when at an already depolarised membrane potential (Surmeier et al., 2007).

For the D2 MSNs, we add dopaminergic modulation of intrinsic ion channels by extending (2) to

$$C\dot{v}_{D2} = k(1 - \alpha\phi_2)(v_{D2} - v_r)(v_{D2} - v_t) - u + I, \quad (5)$$

where we only decrease k by a factor of $(1 - \alpha\phi_2)$, which is sufficient to model the increased sensitivity to injection current following D2 activation (Moyer et al., 2007).

We model synaptic input to all the MSNs as

$$I = I_{\text{ampa}} + B(v)I_{\text{nmda}} + I_{\text{gaba-fs}} + I_{\text{gaba-ms}}, \quad (6)$$

where both I_{ampa} and I_{nmda} are derived from cortical input, $I_{\text{gaba-fs}}$ from FSI input, and $I_{\text{gaba-ms}}$ from local MSN collaterals. Each synaptic input of type z (ampa, nmda, gaba-fs, gaba-ms) is modelled by

$$I_z = \bar{g}_z h_z (E_z - v), \quad (7)$$

Table 2

Intrinsic and synaptic parameters for the medium spiny neuron model. Dimensions are given where applicable.

Parameter	Value	Source
C	50 pF	Izhikevich (2007)
b	−20	"
c	−55 mV	"
v_r	−80 mV	"
v_{peak}	40 mV	"
k	1.14	Humphries et al. (submitted for publication)
v_t	−33.8 mV	"
a	0.05	"
d	377	"
α	0.03	"
g_{DA}	22.7 nS	"
E_{DA}	−68.4 mV	"
β_1	3.75	"
β_2	0.156	"
$E_{\text{ampa}}, E_{\text{nmda}}$	0 mV	Moyer et al. (2007)
$E_{\text{gaba-fs}}, E_{\text{gaba-ms}}$	−60 mV	"
τ_{ampa}	6 ms	"
τ_{nmda}	160 ms	"
$\tau_{\text{gaba-fs}}, \tau_{\text{gaba-ms}}$	4 ms	"
g_{ampa}	6.1 nS	Humphries et al. (submitted for publication)
g_{nmda}	3.05 nS	"
$g_{\text{gaba-ms}}$	4.36 nS	"
$g_{\text{gaba-fs}}$	21.8 nS	~ 5 × MSN conductance Koos et al. (2004)
$[\text{Mg}^{2+}]_0$	1 mM	Jahr and Stevens (1990)

where \bar{g}_z is the maximum conductance and E_z is the reversal potential. We use the standard single exponential model of post-synaptic currents

$$\dot{h}_z = \frac{-h_z(t)}{\tau_z}, \quad \text{and} \quad h_z(t) \leftarrow h_z(t) + S(t)/\tau_z, \quad (8)$$

where τ_z is the appropriate synaptic time constant, and $S(t)$ is the number of pre-synaptic spikes arriving at all the neuron's receptors of type z at time t . Finally, we have the term $B(v)$ that models the voltage-dependent magnesium plug in the NMDA receptors (Moyer et al., 2007)

$$B(v) = \frac{1}{1 + \frac{[\text{Mg}^{2+}]_0}{3.57} \exp(-v \cdot 0.062)}, \quad (9)$$

where $[\text{Mg}^{2+}]_0$ is the equilibrium concentration of magnesium ions.

We add D1 receptor dependent enhancement of NMDA-evoked EPSPs (Moyer et al., 2007) by

$$I_{\text{nmda}}^{\text{D1}} = I_{\text{nmda}}(1 + \beta_1 \phi_1), \quad (10)$$

and we add D2 receptor dependent attenuation of AMPA-evoked EPSPs (Moyer et al., 2007) by

$$I_{\text{ampa}}^{\text{D2}} = I_{\text{ampa}}(1 - \beta_2 \phi_2), \quad (11)$$

where β_1 and β_2 are scaling coefficients determining the relationship between dopamine receptor occupancy and the effect magnitude. All parameter values are given in Table 2.

3.1.2. Dopamine-modulated FSIs

The FSIs only express the D1-family of receptors on their membranes (Centonze et al., 2003). We add D1-receptor modulation by extending (2) to

$$C \dot{v}_{\text{fs}} = k[v_{\text{fs}} - v_r(1 - \eta \phi_1)](v_{\text{fs}} - v_t) - u_{\text{fs}} + I, \quad (12)$$

where we increase the nominal resting potential v_r by a factor of $(1 - \eta \phi_1)$, following experimental data from Bracci, Centonze, Bernardi, and Calabresi (2002) and Centonze et al. (2003).

Table 3

Intrinsic and synaptic parameters for the fast spiking interneuron model. Dimensions are given where applicable. n.d.: no data.

Parameter	Value	Source
a	0.2	Izhikevich (2007)
b	0.025	"
d	0	"
k	1	"
v_{peak}	25 mV	"
v_b	−55 mV	"
C	80 pF	Tateno et al. (2004)
c	−60 mV	"
v_r	−70 mV	"
v_t	−50 mV	"
η	0.1	fitted to Bracci and Panzeri (2006)
ϵ	0.625	fitted to Gorelova et al. (2002)
$E_{\text{ampa}}, E_{\text{nmda}}$	0 mV	n.d.; set as for MSNs
$E_{\text{gaba-fs}}, E_{\text{gaba-ms}}$	−60 mV	"
τ_{ampa}	6 ms	"
$\tau_{\text{gaba-fs}}$	4 ms	"
g_{ampa}	61 nS	n.d.; tuned to achieve realistic firing rates (Section 5.2)
$g_{\text{gaba-fs}}$	20 nS	n.d.; assumes equivalent effect of FSI-FSI contacts as FSI-MSN contacts (Section 3.1.3)
g	30 nS	"
τ	11 ms	"

Following Izhikevich (2007), we use a nonlinear u term

$$\dot{u}_{\text{fs}} = \begin{cases} -au_{\text{fs}}, & \text{if } v_{\text{fs}} < v_b, \\ a[b(v_{\text{fs}} - v_b)^3 - u_{\text{fs}}], & \text{if } v_{\text{fs}} \geq v_b, \end{cases} \quad (13)$$

that enables the FSI model to show Type 2 dynamics, particularly a non-linear step at the start of its current-frequency curve from 0 to around 15–20 spikes/s.

Synaptic input to the striatal FSIs predominantly activates GABAa or AMPA receptors (Blackwell, Czubayko, & Plenz, 2003), NMDA receptors are rare. The dendrodendritic gap junctions provide a further source of “synaptic” current (Koos & Tepper, 1999). Thus the synaptic current contributions are

$$I = I_{\text{ampa}} + I_{\text{gaba}}^* + I_{\text{gap}}, \quad (14)$$

where we add D2-receptor dependent modulation of GABAergic input (Bracci et al., 2002; Centonze et al., 2003) by

$$I_{\text{gaba}}^* = I_{\text{gaba}}(1 - \epsilon \phi_2), \quad (15)$$

where I_{gaba} is derived from FSI input. All parameter values are given in Table 3.

3.1.3. Tuning FSI gap junctions

A gap junction between FSIs i and j is modelled as a compartment with voltage v_{ij}^* , which has dynamics

$$\tau \dot{v}_{ij}^* = (v_i - v_{ij}^*)(v_j - v_{ij}^*), \quad (16)$$

where τ is a time constant for voltage decay, and v_i and v_j are the membrane potentials of the FSI pair. The current introduced by that cable to the FSI pair is then

$$I_{\text{gap}}^*(i) = g(v_{ij}^* - v_i) \quad I_{\text{gap}}^*(j) = g(v_{ij}^* - v_j), \quad (17)$$

where g is the effective conductance of the gap junction. The total gap junction input I_{gap} to an FSI is then the sum over all contributions I_{gap}^* .

We hand-tuned τ and g using a pair of FSI models connected by a gap junction. Our target data came from a study by Galarreta and Hestrin (1999), in which a sinusoidal current at different frequencies was injected into one of a gap-junction coupled pair of cortical FSIs, and membrane voltages recorded from both: this data is ideal as it provides both voltage coupling strength and voltage phase-lag, which are affected by both g and τ . We injected

Fig. 3. Tuning the gap junction model. Galarreta and Hestrin (1999) injected a sinusoidal current into a cortical FSI at various frequencies, and recorded from another connected to it by a gap junction. They computed both the coupling ratio (■) and phase lag (●) of the second neuron's membrane potential with respect to the injected neuron. We similarly connected a pair of model FSIs with our gap junction model, injected a sinusoidal current into one, and hand-tuned the gap junction parameters (g and τ) to fit the data. A qualitatively good match was achieved by the model for both coupling ratio (□) and phase lag (○).

a sinusoidal current I into one FSI with an amplitude of 400 pA at different frequencies and computed the coupling coefficient (ratio of maximum amplitudes in the membrane voltages of the two neurons) and the phase-lag (voltage-peak offset as a function of the injection current frequency). Fig. 3 shows we achieved a good qualitative match to both coupling coefficient and phase-lag from the experimental data, with $\tau = 11$ ms and $g = 150$ nS.

While this data-set was the most appropriate for tuning the gap junction model, we cannot immediately use the value for g . Two caveats have to be accounted for: first, that there is an unknown number of other FSIs connected by gap junctions to the studied pair; second, that the study was done in tissue from juvenile rats, and so would over-express gap junctions (Belluardo et al., 2000). Both of these would contribute to the decay of the coupling coefficient. Thus, we find we need to re-scale g to account for the approximate reduction in gap junctions in adult tissue and to account for other connections. In further simulations we explored fully-connected gap-junction networks of 3, 4 or 5 FSIs, as might be found in juvenile tissue. We found that repeating the same paired recording protocol in these networks did indeed predict a dramatic reduction in g : the multiple gap junctions acted to reinforce the effects of the injection current on the un-injected neuron. A five-fold reduction to $g = 30$ nS produced an equivalent fit to the data in Fig. 3 for all three networks, and so we used that figure here. This is also consistent with the comparatively weak coupling coefficients of 3% and 20% that have been reported for the few gap junction coupled striatal FSIs recorded to date (Koo & Tepper, 1999).

3.2. Input to network

In addition to its synaptic connections defined by our network model, each neuron received an external input representing its cortical afferents. In many spiking neuron models, afferent input is generated by a set of Poisson processes. However, for large-scale models where each neuron receives hundreds or thousands of afferent inputs, this becomes unfeasible because of the memory requirements. Recently we have developed a series of tools addressing just this problem, using a method that collapses many afferent trains into an single equivalent spike-event count.

Each spike-event generator directly produces the spike-events that occur across N afferents to the neuron. At each time-step Δt , and given a mean spike rate r , we compute the probability of a spike per afferent as $p(s) = r\Delta t$. The total number of spike-events

S at each time-step is then just drawn from a binomial distribution $S = B(N, p(s))$. The resulting time-series of spike-events is equivalent to the pooling of N spike trains modelled as independent renewal processes, the superset that includes Poisson processes.

We define N and r for the striatal network for the tonic background *in vivo* state, by combining data from anatomy and electrophysiology:

1. In a recent organotypic cortico-striatal-nigral co-culture study, Blackwell et al. (2003) reported that a striatal MSN receives an average of around 800 synaptic events per second during its depolarised (“up”) state, but they could not distinguish excitatory and inhibitory potentials.
2. The ratio of asymmetric (putative excitatory):symmetric (all others) synapses in rat striatum is $\sim 3.9:1$ (Ingham, Hood, Taggart, & Arbuthnott, 1998).
3. If we conservatively assume that half the asymmetric synapses are cortical in origin, then we have a ratio of 2:1 potentially active synapses in the co-culture.
4. Assuming this corresponds (roughly) to the proportion of glutamate:GABA activity, then cortical activity accounts for ~ 530 synaptic events per second.
5. Given the estimate of 4250 cortical inputs per MSN (Zheng & Wilson, 2002), the average firing rate of those cortical neurons is therefore ~ 0.12 spikes/s.
6. From *in vivo* extracellular recordings, we know that dedicated cortico-striatal neurons tonically fire a maximum of 5 spikes/s and pyramidal tract neurons with striatal collaterals tonically fire around 15 spikes/s (Bauswein, Fromm, & Preuss, 1989; Turner & DeLong, 2000). The former dominate in number over the latter (Bauswein et al., 1989; Zheng & Wilson, 2002), suggesting an overall mean rate around 2–5 spikes/s.
7. Taking the lower mean single neuron rate of 2 spikes/s, and the estimate of 530 synaptic events per second, we see that just 265 active cortico-striatal neurons are required to achieve this — or just 6% of the total afferent cortical population.

Overall then, tonic cortico-striatal activity sufficient to drive MSN firing requires just $N \simeq 250$ trains, at a rate of $r \simeq 2$ spikes/s. We hence use $N = 250$ and $r = 1.9$ spikes/s for the MSN input throughout our simulations. In addition, we use the same N, r in the spike-event generators for the FSIs, as there is no data on cortical input to these neurons.

4. Detecting groups of synchronised cells in multi-unit data

We sought to identify potential candidates for the basic computational elements of the striatum from the dynamics of our large-scale models under background input. For our present purposes, we wanted to find groups of co-active or mutually antagonistic MSNs that could form the basis for competitive dynamics within the striatum. In addition, we studied this input regime to see if the reported striatal cell clusters, spontaneously formed *in vitro* (Carrillo-Reid et al., 2008), could be identified in our model. However, analysis methods suitable for exploratory analysis of such large spike-train data-sets are lacking (Brown, Kass, & Mitra, 2004). We therefore developed a new algorithm for finding synchronised groups at multiple time-scales within a multiple spike-train data-set.

At its most general, our algorithm follows a two-step procedure. First, some measure of correlation between each pair (or more) of neurons is computed, resulting in a correlation matrix. Second, some method acts on this matrix to identify “strong” spike-train correlations within *groups* of neurons, thereby grouping the data-set into sets of neurons whose output is more related to each other than with the remaining neurons. A group is thus 3 or more neurons that are co-correlated. With this in mind, we detail our specific algorithm (our present choices for these two steps are specified in the Appendix):

